Benchmarking the dynamics of phosphatidylcholine headgroup and glycerol backbone molecular dynamics models using open data

Hanne S. Antila,[†] Tiago Ferreira,[‡] Matti Javanainen,[¶] O. H. Samuli Ollila,[§] and Markus Miettinen[*,†]

[†]*Department of Theory and Bio-Systems, Max Planck Institute of Colloids and Interfaces, 14476 Potsdam, Germany*
[‡]*Tiago's affiliation here*
[¶]*Add Matti to author list?*
[§]*Samuli's affiliation here*

E-mail: markus.miettinen@mpikg.mpg.de

Abstract

Brilliant abstract here

1 Introduction

Phospholipids are an important class of biomolecules not only as the building blocks of biomembranes but also as emerging candidates for micro- and nanotechnology, such as the use of liposomes as microcapsules in targeted drug delivery.[1] These molecules are composed of a hydrophilic phosphate head group, which is connected to two hydrophopic fatty acid tails via a glycerol backbone. The ability of lipids to self assemble into bilayer membrane (and other) configurations is a direct consequence of this dual nature and the conformations adopted by the molecules play a crucial in role in determining properties of these lipid assemblies, such as the dipole potential[2] and the curvature? **1.Markus, any favourite references on curvature?**

Although biological membranes are complex mixtures of multiple different lipids as well as other molecules, lamellar phospholipid bilayers with one or few lipid types have been successfully used as simplified models systems to decipher, *eg.*, possible molecular mechanisms behind anesthetics,[3?] the effect of cholestherol on membrane structure,[4?] and the functioning of membrane proteins[5] **2.Markus, do you want to add your favourite topics/references, espc. experimental**. The ability of the simple model membranes to reproduce the biological functioning of headgroup/glycerol structure in cells is backed up by experimental evidence.[6] In particular, classical molecular dynamics (MD) simulations of these model systems have been widely utilized[3,4,7? –10] to provide an atomistic view on the biomembranes, and hold vast potential in making further connections between the structure and the function.

Unfortunately, recent comparison of lipid order parameters from bilayer simulations to nuclear magnetic resonance (NMR) measurements have showed that none of the currently available lipid MD models (force fields) perfectly reproduces the conformational ensemble sampled by the headgroup.[8] Here, we take a step further and investigate the dynamics of those MD models. Our motivation is two-fold. Firstly, when investigating static properties of the bi-

layers, it is crucial to assess how well the simulations have converged. In order to extract reliable statistics, the conformations sampled has to represent the equilibrium distribution with enough transitions between states. Indeed, simulations of a single (1,2-Dioleoyl-sn-glycero-3-phosphocholine) DOPC lipid using the CHARMM32b2 force field indicated that the conformations sampled do not replicate the equilibrium distribution even after 500 ns[11] and bond dynamics of the Berger model was shown[9] to be too slow at the glycerol region of 1-Palmitoyl-2-oleoylphosphatidylcholine (POPC) compared to correlation times extracted from NMR experiments. Secondly, for complete picture of membrane functioning, knowledge on the bilayer dynamics in addition to equilibrium measurements are needed. The ability of the MD model to reproduce the relative abundance of different dynamical processes is crucial for the correct interpretation of pathways leading to, eg., membrane deformation[12] and lipid-induced conformational[13,14] changes of membrane proteins.

Both the conformational dynamics of lipids in experimental bilayers[15–19] and the dynamics produced by lipid MD models in bilayer simulations[15,17,18,20] have been traditionally assessed based on the spin-lattice relaxation rates R_1 (or the corresponding T_1 times), available through NMR measurements. At best, the simulation can be combined with the NMR experiments to provide an interpretation of the molecular motion.[18,20,21] However, relying on R_1 only has several drawbacks **3.do all flavors (31P,13C,...) have the same problem?**. It builds on an underlying rotation-diffusion model, its sensitivity is typically limited to C–H bond reorientation with time scales ∼1-10 ns, and measurements at several temperatures and magnetic field strengths are required to fully characterize the dynamics. To address these deficiencies, two of us introduced a procedure for quantifying[9] the effective C–H correlation times (τ_e)—a model free quantity that encompasses conformational dynamics with time scales up to hundreds of nanoseconds—from bilayer systems. Most importantly, increasing τ_e always signals some type of slowdown in the C–H bond dynamics, making the interpretation less ambiguous than for R_1, where slowdown in the dynamics can lead to either an increase or a decrease of R_1 value.[9]

Here, we utilize the effective correlation time to present the first comprehensive comparison of dynamics of 1-Palmitoyl-2-oleoylphosphatidylcholine (POPC) in different MD models. We not only investigate the pure bilayers in room temperature but also explore the effect of cholesterol content, hydration and monovalent salt to see whether the model dynamics correctly responds to the change in conditions. An MD model fulfilling these requirements can provide a reliable tool to study, *eg*, membrane remodeling, or to interpret the experimental spin relaxation rates by connecting them to the underlying dynamical processes.

Within this study, we intentionally restrict ourselves to re-use existing, publicly available simulation trajectories. This is to demonstrate the power of open, well documented data in creating new knowledge at a lowered cost. The project was conducted as a open collaboration under the NMRlipids (`nmrlipids.blogspot.fi`) open science project and the main source of data was the collection of lipid bilayer simulations originating from the previous NMRlipids projects.[8,22]

2 Methods

3 Theoretical background

The ^{13}C NMR experiments investigating the lipid conformational dynamics take advantage of the fact that the relaxation of ^{13}C magnetization dominantly happens via the dipolar coupling of the carbon with the magnetic moments of the protons bound to it, with the symmetry axis of the interaction aligning with the C–H bond. The spectral density depicting the ^{13}C relaxation rates (at frequency ω) is expressed as

$$\mathrm{j}(\omega) = 2\int_0^\infty \cos(\omega\tau)\mathrm{g}(\tau)d\tau, \qquad (1)$$

which is the Fourier transformation of the C–

H bond second order autocorrelation function at time τ

$$\mathrm{g}(\tau) = \langle P_2\left[\vec{\mu}(t)\cdot\vec{\mu}(t+\tau)\right]\rangle, \qquad (2)$$

where $\vec{\mu}(t)$ is the unit vector in the direction of the C–H bond at time t and P_2 is the second order Legendre polynomial. The angular brackets depict averaging over time. The autocorrelation function can be expressed as the product of two functions

$$\mathrm{g}(\tau) = \mathrm{g_f}(\tau)\mathrm{g_s}(\tau), \qquad (3)$$

where $\mathrm{g_f}(\tau)$ characterizes fast decays owing to, for example, the molecular rotations, and $\mathrm{g_s}(\tau)$ describes slow decays that originate from, *eg.*, the lipid diffusion. The two components, along with the oscillation due to magic angle spinning at the ∼kHz region, are depicted in Fig. 1. Correlation time of 4.2 ms has been estimated for multilamellar POPC samples at 300 K for the slow modes, whereas in liquid crystalline lipid bilayers the faster $\mathrm{g_f}(\tau)$ decays to a plateau value S^2_{CH} within few hundred nanoseconds.[9] The order parameters

$$S_{\mathrm{CH}} = \frac{1}{2}\langle 3\cos^2\theta - 1\rangle, \qquad (4)$$

where θ is defined as the angle between the C–H bond and the bilayer normal, are measured in NMR experiments from this plateau. As S_{CH} describes the conformational ensemble of the molecule, the fast-decaying component of the rotational correlation function intuitively depicts the time needed to sample these conformations. The characteristic time can be quantified via the effective correlation time

$$\tau_e = \int_0^\infty \frac{\mathrm{g_f}(\tau) - S^2_{\mathrm{CH}}}{1 - S_{\mathrm{CH}}} d\tau \qquad (5)$$

which is defined via the area of the normalized correlation function ($\mathrm{g_f'}(\tau) = \mathrm{g_f}(\tau) - S^2_{\mathrm{CH}}/1 - S_{\mathrm{CH}}$) and graphically depicted in Fig. 1b. It is easily seen that in the presence of more long-lived correlations τ_e grows, signaling that more time is needed for full conformational sampling.

The bond correlation functions are easily accessible from MD simulations. In addition to extracting τ_e directly from the area, fitting a

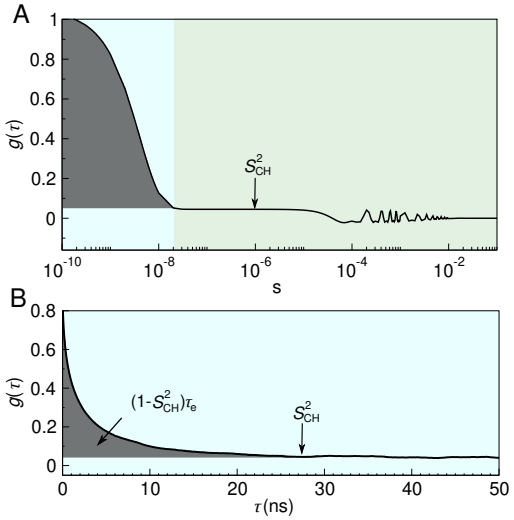

Figure 1: The autocorrelation function $g(\tau)$ a) The fast mode (shaded blue) and the slow mode (shaded green) of the correlation function along with the oscillation owing to magic angle spinning. The fast mode decays to plateau quantifying the S_{CH} while the slow mode gives the final descent to zero. b) Illustration of typical autocorrelation function obtained from a MD simulation. The gray area under the curve gives means of quantifying the τ_e.

set of N exponentials, each with their own correlation times τ_i to the normalized correlation function

$$\mathrm{g'_{MD}}(t) = \sum_{i=1}^{N} \alpha_i e^{-t/\tau_i} \qquad (6)$$

provides an alternative way of quantifying τ_e

$$\tau_e = \sum_{i=1}^{N} \alpha_i \tau_i. \qquad (7)$$

When the simulation trajectory is not long enough for the correlation function to reach the plateau, calculating the area gives a lower bound estimate for τ_e while the latter method includes also contribution from the longer-time components via the fitting process. However, in practice the fit is often highly unreliable in terms of depicting the long tails of the correlation function, and in this work we choose to quantify τ_e using the area.

The spin-lattice relaxation rate R_1 defines the time-scale on which ^{13}C longitudal magnetiza-

tion equilibrates. It is defined as

$$R_1 = \frac{d_{\mathrm{CH}} N_{\mathrm{H}}}{20} \left[j(\omega_{\mathrm{H}} - \omega_{\mathrm{C}}) + 3j(\omega_{\mathrm{C}}) + 6j(\omega_{\mathrm{H}} + \omega_{\mathrm{C}}) \right], \tag{8}$$

where N_{H} is the number of bound hydrogens, ω_{H} and ω_{C} are the Larmor frequencies for ^{1}H and ^{13}C, and d_{CH} is the rigid dipolar coupling constant. For the methylene bond, $d_{\mathrm{CH}}/2\pi$ approximately equals to -22kHz.

The dependency of R_1 on the spectral density values at the Larmor frequencies means that the R_1 value depicts the relative amounts of relaxation processes with time-scales near the inverses of these frequencies. Since the Larmor frequencies depend on the field strength used in the NMR measurements, this typically makes R_1 sensitive to ∼1-10 ns time-scales. Importantly, a change in R_1 indicates a difference in the relative amount of processes within the detection window, and therefore does not give information on the modulation of the total sampling rate.

3.1 Data aquisition

The simulation trajectories used in this work were collected from the Zenodo repository `zenodo.org` **4.is this the best way to cite Zenodo?**. A List of the simulations, as well as the references to the data files are presented in Table 1 for trajectories near room temperature and in full hydration, Table 2 for simulations including cholesterol, Table 3 for data under varying hydration, and Table 4 for simulations in increasing NaCl concentration. Additional computational details of each of the simulations are available at the referred Zenodo entry. All the experimental quantities were collected from the literature **5.except are they, or mostly from Tiago?** sources referred at the respective figures**6.how to refer to experimental data**.

The project was conducted as open collaboration using the `nmrlipids.blogspot.fi` blog as a communication platform. An open invitation to contributions was presented in the blog, and every contributor was offered a co-authorship. The input from each author is detailed in XXX **7.acknowledgements? SI?**. **8.Currently all simulation data was extracted from the zenodo repository, including Berger data (not from the 2015 paper)**

Table 1: Simulations of POPC bilayers under full hydration. Number of lipids and number of water molecules are denoted with N_l and N_w, respectively, temperatures (T) are given in kelvins and t_{anal} is the length of the trajectory used for analysis. The column labeled "Files" lists links for the downloadable simulation files.

Force field	lipid	N_l	N_w	T (K)	t_{anal} (ns)	Files
Berger-POPC-07[23]	POPC	128	7290	298	50	[24]
CHARMM36[25]	POPC	128	5120	303	140	[26]
CHARMM36[25]	POPC	17	510	300	140	[27]
MacRog[28]	POPC	128	6400	310	400	[29]
Lipid14[30]	POPC	72	2234	303	50	[31]
Slipids[32]	POPC	200	9000	310	500	[33]

Table 2: Simulation data for cholesterol-containing POPC bilayers. Number of cholesterols is given by N_{chol} while C_{CHOL} denotes the percentage of cholesterol from all the lipids. Rest of the labels are as in Table 1.

Force field	lipid	N_l	N_{chol}	C_{CHOL}	N_w	T (K)	t_{anal} (ns)	Files
Berger-POPC-07[23]	POPC	128	0	0%	7290	298	50	[24]
/Höltje-CHOL-13[4,34]	POPC	64	64	50%	10314	298	60	[35]
CHARMM36[25,36]	POPC	128	0	0%	5120	303	140	[26]
	POPC	80	80	50%	4496	303	200	[37]
MacRog[28]	POPC	128	0	0%	6400	310	400	[29]
	POPC	64	64	50%	6400	310	400	[29]
Slipids[32,38]	POPC	200	0	0%	9000	310	500	[33]
	POPC	200	200	50%	18000	310	500	[33]

Table 3: Simulation data for bilayers under varying hyration level. The water to lipid ratio is denoted as W/L, and other labels are as in Table 1.

Force field	lipid	(W/L)	N_l	N_w	T (K)	t_{anal} (ns)	Files
Berger-POPC-07[23]	POPC	57	128	7290	298	50	[24]
	POPC	7	128	896	298	60	[39]
Berger-DLPC-13[40]	DLPC	16	72	1152	300	80	[41]
	DLPC	12	72	864	300	80	[42]
CHARMM36[25]	POPC	40	128	5120	303	140	[26]
	POPC	15	72	1080	303	20	[43]
	POPC	7	72	504	303	20	[44]
MacRog[28]	POPC	50	288	14400	310	40	[45]
	POPC	15	288	4320	310	100	[45]
	POPC	10	288	2880	310	100	[45]

4 Results

Figure 2 presents a comparison of experimental effective correlation times, obtained from

Table 4: Simulation data for bilayers under varying concentration of NaCl. Number of Na^+ and Cl^- ions are denoted by N_{Na} and N_{Cl} while [salt] gives the NaCl concentration calculated as [salt] $=N_{Na}$[water]$/N_w$, where [water] = 55.5 M. Other labels are as in Table 1.

Force field (lipid, ion)	lipid	[salt] mM	N_l	N_w	N_{Na}	N_{Cl}	T (K)	t_{anal} (ns)	Files
CHARMM36[25]	POPC	0	128	5120	0	0	303	140	[26]
CHARMM36,[25] CHARMM36[46]	POPC	350	72	2085	13	13	303	80	[47]
CHARMM36,[25] CHARMM36[46]	POPC	690	72	2085	26	26	303	73	[48]
CHARMM36,[25] CHARMM36[46]	POPC	950	72	2168	37	37	303	60	[49]
MacRog[28]	POPC	0	128	6400	0	0	310	400	[29]
MacRog,[28] OPLS[50]	POPC	100	288	14554	27	27	310	90	[51]
MacRog,[28] OPLS[50]	POPC	210	288	14500	54	54	310	90	[51]
MacRog,[28] OPLS[50]	POPC	310	288	14446	81	81	310	80	[51]
MacRog,[28] OPLS[50]	POPC	420	288	14392	108	108	310	90	[51]
Slipids[32]	POPC	0	200	9000	0	0	310	500	[33]
Slipids,[32] AMBER[52]	POPC	130	200	9000	21	21	310	100	[53]
Slipids,[32] AMBER[52]	POPC	1.0	200	900	162	162	310	200	[54]

POPC bilayers in room temperature and under full hydration, to those produced by five different MD force fields. In general, MD models exhibit a tendency towards slower dynamics than what is observed experimentally in the headgroup and glycerol region, while the dynamics of the tail C–H bonds are well reproduced. The discrepancy is most drastic in the glycerol region of the molecule which is consistent with previous results from the Berger model,[9] as well as the insufficient conformational sampling of glycerol backbone torsions observed[11] in 500ns-long CHARMMc32b2[55,56] simulations of a DOPC lipid. The best overall performance is obtained from CHARMM36 and Slipids force fields, although Slipids model dynamics exhibits a qualitatively wrong, decreasing trend from g_3 to g_1. **9.not extremely clear, though**.

Note that for an united atom mode (such as Berger model studied here) the hydrogens are added to the trajectory after the simulation and the dynamics are not preserved for the methyl C–H bonds by the protonation algorithm. Hence, the data for the γ, oleoyl C18, and palmitoyl C16 carbons from the Berger model are not presented. Furthermore, the values calculated from the simulations give the lower limit of τ_e, as we opted to quantify these from the area (see section 3), and the overestimation of the effective correlation time for some models might be more severe than what is shown here.

In Figure 2 we also provide a comparison of experimental R_1 rates to those obtained from the simulations, under the same conditions as for τ_e. In contrast to the τ_e values, the force fields overall reproduce the experimental R_1 data well the glycerol and headgroup region **12.what is up with the gamma carbons?**. The Lipid14 model produces particularly good results whereas CHARMM36 force field exhibits tendency towards faster dynamics than what is observed experimentally. Based on the ability of the MD models to represent the R_1 rates, and the discrepancies observed for τ_e data, we conclude that the force fields tend to reproduce the dynamics at $\sim$1 ns scales for the glycerol region but differences arise in longer processes contained in the τ_e values.

In the tail region the MD models are overall good in agreement with R_1 rates. The Slipids and Berger model are usually underestimating the experimental value, whereas the Lipid14 mostly produces the fastest rates of all the models. The good agreement obtained for R_1 values shows that MD models are able to replicate the dynamical processes of tail C–H bonds at the effective correlation times $\sim$1 ns scales whereas the ability to reproduce the effective correlation times (Fig. 2) confirms that the overall dynamics are accurate, and possibly indicates that the $\sim$1 ns scales processes are dominant in the tail region.

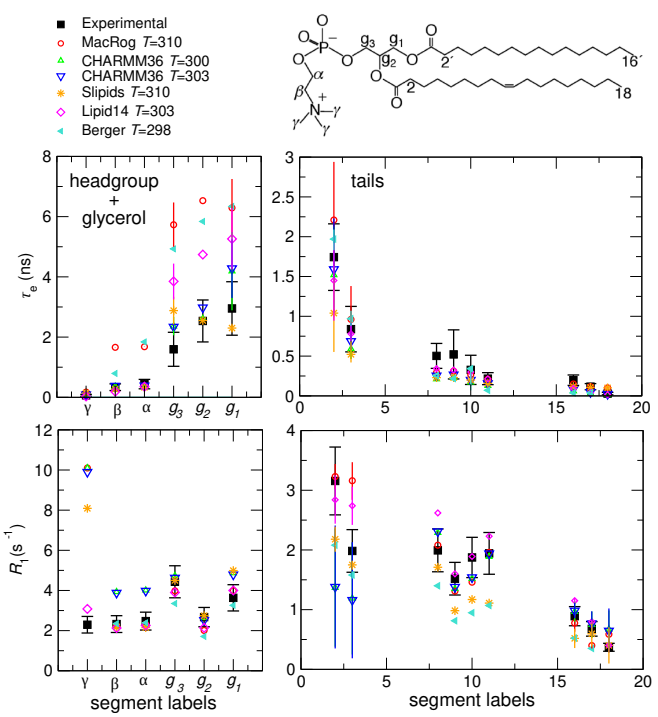

Figure 2: Comparison of experimental effective correlation times (τ_e) and R_1 rates to those obtained from MD simulations of POPC bilayers under full hydration. The structure of POPC along with the the carbon labelling scheme is presented on the top. The experimental values are measure from fully hydrated POPC bilayers in L_α phase at 298 K. The data for segment 8–11 is from the sn-2 (oleoyl) chain, whereas non-resolved contributions from both acyl chains are included in segments 2–3 and 16–18 (14–16 for sn-1 chains). The error bars for experimental values reflect error estimate of XXX, whereas the bars for simulated data points give the minimum and maximum value observed at each carbon while the symbol denotes the average. For the simulated data this includes contributions from both chains for carbon labels 2–3 and 16–18, in line with the experimental data. Further details on the simulations are provided in Table 1.

10.error estimate has changed 11.how to refer to experiment

A comparison to experiments under one set of conditions is not sufficient to fully assess the quality of the dynamics obtained from an MD model: a more complete picture is acquired by evaluating whether the model responds correctly to the change in conditions. We therefore proceed to investigate how the dynamics change when cholesterol is added to the bilayer (Fig. 3), when the hydration level is reduced (Fig. 4) and when monovalent salt is added to the solution (Fig. 5).

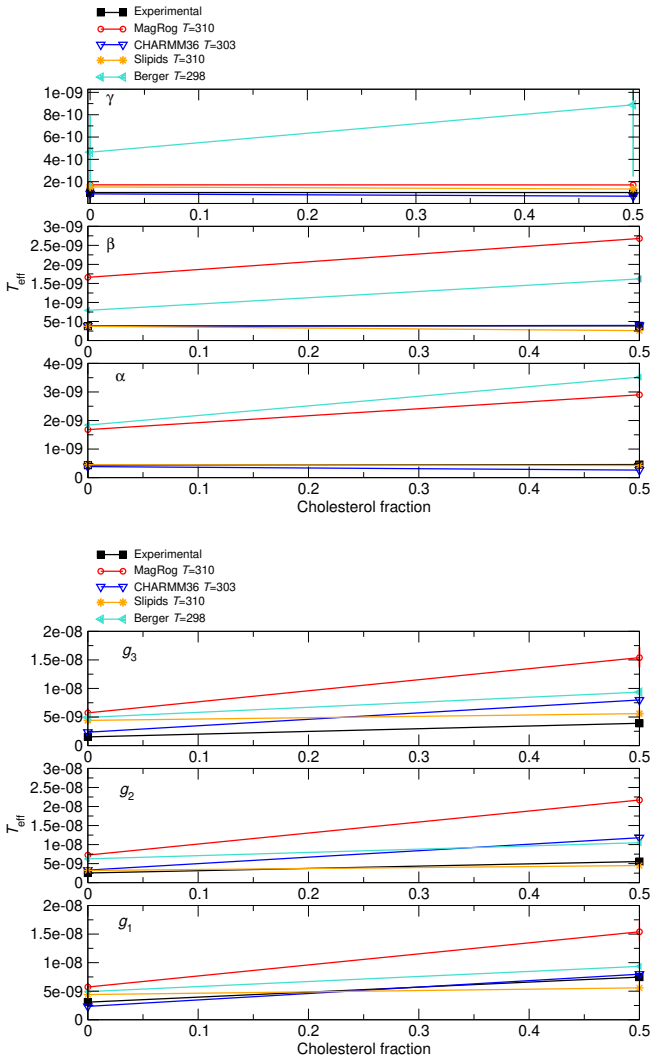

Figure 3: The effect of bilayer cholesterol content. The experimental values are from XXX and measured at XXXK. Further details on the simulations are provided in Table 2.

13.updated cholesterol data needed, remove berger datapoints for gamma, as for delta teff

Experimentally, additional cholesterol is know to cause slower decorrelations of the hydrogens attached to POPC g_1, g_2, and g_3 carbons. All the force fields investigated in Fig. 3 qualitatively reproduce this. The increase upon addition of cholesterol is overestimated with the MacRog and CHARMM36 models while slight

underestimation occurs when using Slipids and Berger force fields, especially at g_1 and g_2 carbons. The change observed here, however, is particularly sensitive to the length of the trajectory as cholesterol-induced increase in effective correlation time is likely to lead to worse convergence of the correlation function within the limited simulation time, and more drastic underestimation of τ_e is expected than for simulations without cholesterol. This will, consequently, cause a tendency towards underestimation on the strength of the cholesterol-driven modulation of the effective correlation time. For the α , β, and γ carbons no change in τ_e is detected experimentally. Nevertheless, Berger and MacRog models exhibit a slow-down in dynamics also for these C–H bonds, while the τ_e in other models remains constant.

To investigate the effect of hydration on the C–H bond dynamics on the PC headgroup, we first present a comparison of experimental effective correlation times obtained from the POPC (measured in full hydration) and DMPC (1,2-Dimyristoyl-sn-glycero-3-phosphocholine, measured in low hydration) in Fig. 4a. The values are the same within the experimental accuracy, which leads to two conclusions, 1) the motions of the headgroup bonds are unaffected by the differences in the tails between the two molecules and 2) the decrease of hydration level down to 13 waters per lipid does not considerably alter the correlation times for the headgroup/glycerol region.

Figure 4b presents effective correlation times obtained from three different MD models as function of reducing hydration. All the force fields produce τ_es that are relatively unaffected by the hydration level above 15 waters per lipid (W/L), in line with the experimental observation. When the hydration is further reduced, the dynamics slows down. The effect is weakest with the CHARMM36 model while more pronounced increase in τ_e is observed with MacRog and Berger force fields. At these same levels of hydration, a change the lipid headgroup order parameters is detected,[8] owing to the tilt of the headgroup towards the tails under low hydration conditions.[?] NMR relaxation time (T_1) measurements from DOPC bilayers[?] have revealed a simultaneous slow-down of the headgroup conformational dynamics, which was attributed to the reduction in available volume for the tilted headgroup. This slow-down is in line with the increased effective correlation times produced by the MD models.

In the tail region dehydration causes a consistent slow-down in the effective correlation times when using the Berger and MacRog models (data not shown). This change is accompanied by and increase in the absolute value of the order parameter, which together with the changes observed in the headgroup orientation and dynamics, may signal an onset of a more comprehensive change in the bilayer structure upon dehydration. **14.Markus, see if formulation ok** together with the slow down indicates the onset of structural transition in the bilayer when the hydration level is reduced.

Finally, we study the response of the MD model dynamics to increasing amounts of monovalent salt. Experimentally, the modulation of α and β carbon order parameters upon increasing ion concentration have been used to quantify the ion binding to the lipid bilayers (the molecular electrometer concept[22,58]). As expected from the uncharged nature, the order parameters are constant for POPC bilayers under NaCl addition in experiments, indicating negligible ion binding. Based on this, we anticipate the correlation times also to be unaffected by monovalent salt but to our knowledge no experimental measurements have been conducted to quantify this.

The molecular electrometer concept has been used to show that most molecular dynamics models overestimate the binding of monovalent ions to the PC headgroup:[22] the modulation the α and β carbon order parameters by increasing NaCl concentration was overestimated compared to the experiments, and accompanied by accumulation of ions at the bilayer surface, in the simulations. In Fig. 5 we compare three force fields, one that is known to exhibit overbinding[22] (MacRog) and two producing more realistic binding affinity (Slipids and CHARMM36). The accumulation of Na^+ ions near the bilayer is quantified in Fig. 5a whereas Fig. 5b shows the chance in τ_e in in-

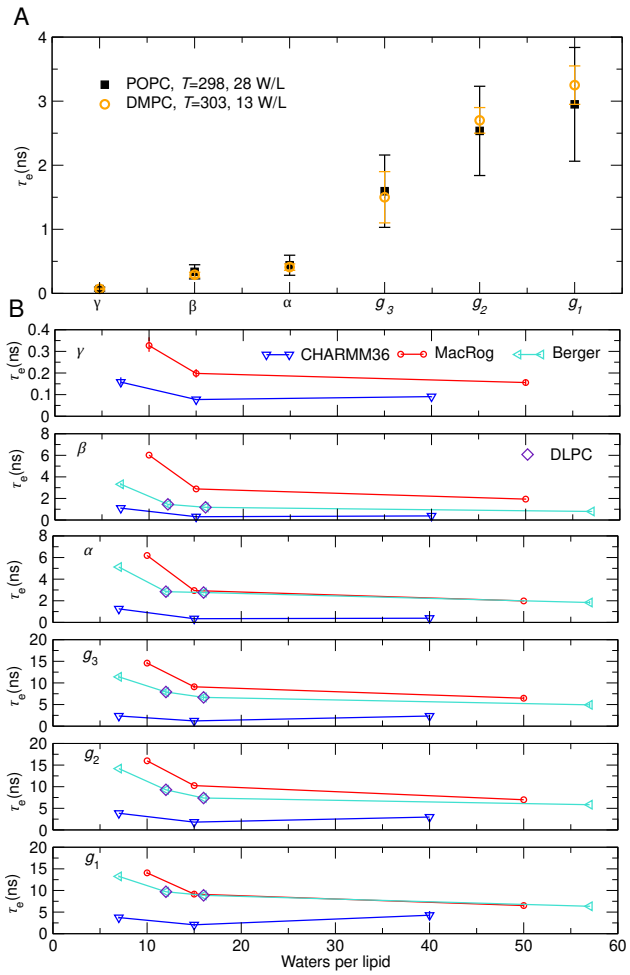

Figure 4: The effect of hydration on the effective correlation times. a) comparison of experimental effective correlation times from DMPC[57] in low hydration (13 W/L) and POPC in full hydration (28 W/L). Neither the different chemistry of the lipid tails, nor the hydration level has an effect within the experimental accuracy. b) The response of effective correlation times to changing hydration level from three MD models. The error bars give the minimum and maximun value observed at each carbon while the symbol denotes the average. Details on the simulations are given in Table 3. Note that two of the data points for the Berger model are from 1,2-didodecanoyl-sn-glycero-3-phosphocholine (DLPC) bilayers (diamonds).

15.how to refer to POPC data

creasing salt concentration. The strength of ion accumulation correlates with the slow down observed in the effective correlation time. Correlation times extracted from the CHARMM36 model vary only a little when ion concentration is increased, whereas a slightly more pronounced change is observed with Slipids and the MacRog model exhibits a clear slow-down. This indicates that, similarly to the order parameters, τ_e may be useful in investigating the ion binding affinity of lipid bilayers.

16.validity of statement regarding Slipids

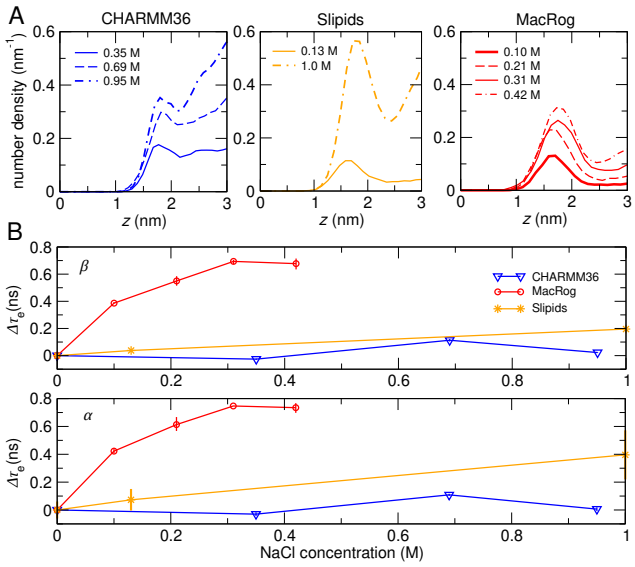

Figure 5: The impact of increasing ionic strength on effective correlation times. a) The density distribution of Na^+ ions as function of distance z from the bilayer center. The plots for each force field are organized from left to right in the order of increasing ion accumulation. b) Effective correlation times for α and β C–H bonds in growing NaCl concentration from CHARMM36, Slipids, MacRog POPC simulations. Details on the simulation data are proviiden in Table 4.

5 Conclusions

Here, we have investigated the dynamics of phosphatidylcholine molecular dynamics models using publicly available MD trajectories. In general, the force fields reproduce the experimentally available R_1 values well, indicating that processes at time scales ∼1 ns are well represented in the MD simulations. That said, comparison to effective correlation times—an experimental measure sensitive to conformational dynamics at a wider range of

time scales—reveals that the MD models are prone to too slow dynamics in the glycerol region. While none of the force fields is able to reproduce all the experimental values, the CHARMM36 POPC model performs well when compared to the effective correlation times, while the Lipid14 force field provides the most realistic R_1 in the PC headgroup and glycerol regions.

We also assessed the how the dynamics of MD models react to the change in conditions; in hydration, cholesterol, and salt content. When reducing the water content, the MD models exhibited somewhat constant correlation times down to ∼15 waters per lipid in agreement with experimental data. After this, a slow down indicative of structural transition was observed. In increasing salt concentration a behaviour reminescent of the molecular electrometer concept was observed: amount of ion binding to the bilayer correlated with the magnitude of slowdown in the correlation times. This opens up the possibility of using effective correlation times in quantifying the ion binding to lipid bilayers. **17.add cholesterol**

Although no new simulations were performed for the purpose of this work, we were able to conduct a comprehensive study on the dynamics of MD models under several conditions. Therefore, this work demonstrates the power of open data in creating new knowledge out of existing trajectories at a reduced cost. If the data is well indexed and documented, this process could be easily automated and has the potential to facilitate faster progress, eg., in the development of MD models.

Acknowledgement

This material is based upon work supported by XXX under Grant No. XXX. The project is/isn't part of the NMRlipids open collaboration (nmrlipids.blogspot.com)

References

(1) Sercombe, L.; Veerati, T.; Moheimani, F.; Wu, S. Y.; Sood, A. K.; Hua, S. Advances and Challenges of Liposome Assisted Drug Delivery. *Frontiers in Pharmacology* **2015**, *6*, 286.

(2) Gawrisch, K.; Ruston, D.; Zimmerberg, J.; Parsegian, V.; Rand, R.; Fuller, N. Membrane dipole potentials, hydration forces, and the ordering of water at membrane surfaces. *Biophysical Journal* **1992**, *61*, 1213 – 1223.

(3) Chau, P.-L.; Hoang, P. N.; Picaud, S.; Jedlovszky, P. A possible mechanism for pressure reversal of general anaesthetics from molecular simulations. *Chemical Physics Letters* **2007**, *438*, 294 – 297.

(4) Ferreira, T. M.; Coreta-Gomes, F.; Ollila, O. H. S.; Moreno, M. J.; Vaz, W. L. C.; Topgaard, D. Cholesterol and POPC segmental order parameters in lipid membranes: solid state 1H13C NMR and MD simulation studies. *Phys. Chem. Chem. Phys.* **2013**, *15*, 1976–1989.

(5) Lindahl, E.; Sansom, M. S. Membrane proteins: molecular dynamics simulations. *Current Opinion in Structural Biology* **2008**, *18*, 425 – 431, Membranes / Engineering and design.

(6) Gally, H. U.; Pluschke, G.; Overath, P.; Seelig, J. Structure of Escherichia coli membranes. Glycerol auxotrophs as a tool for the analysis of the phospholipid headgroup region by deuterium magnetic resonance. *Biochemistry* **1981**, *20*, 1826–1831.

(7) Lyubartsev, A. P.; Rabinovich, A. L. Recent development in computer simulations of lipid bilayers. *Soft Matter* **2011**, *7*, 25–39.

(8) Botan, A.; Favela-Rosales, F.; Fuchs, P. F. J.; Javanainen, M.; Kandu, M.; Kulig, W.; Lamberg, A.; Loison, C.; Lyubartsev, A.; Miettinen, M. S. et al. Toward Atomistic Resolution Structure of Phosphatidylcholine Headgroup and Glycerol Backbone at Different Ambient Conditions. *The Journal of Physical Chem-*

istry B **2015**, *119*, 15075–15088, PMID: 26509669.

(9) Ferreira, T. M.; Ollila, O. H. S.; Pigliapochi, R.; Dabkowska, A. P.; Topgaard, D. Model-free estimation of the effective correlation time for CH bond reorientation in amphiphilic bilayers: 1H13C solid-state NMR and MD simulations. *The Journal of Chemical Physics* **2015**, *142*, 044905.

(10) Miettinen, M. S.; Lipowsky, R. Bilayer membranes with frequent flip-flops have tensionless leaflets. *Nano letters* **2019**, *?*, ?–?

(11) Vogel, A.; Feller, S. E. Headgroup Conformations of Phospholipids from Molecular Dynamics Simulation: Sampling Challenges and Comparison to Experiment. *The Journal of Membrane Biology* **2012**, *245*, 23–28.

(12) Chernomordik, L. V.; Kozlov, M. M. Mechanics of membrane fusion. *Nature structural & molecular biology* **2008**, *15*, 675.

(13) Gibson, N. J.; Brown, M. F. Lipid headgroup and acyl chain composition modulate the MI-MII equilibrium of rhodopsin in recombinant membranes. *Biochemistry* **1993**, *32*, 2438–2454, PMID: 8443184.

(14) Phillips, R.; Ursell, T.; Wiggins, P.; Sens, P. Emerging roles for lipids in shaping membrane-protein function. *Nature* **2009**, *459*, 379.

(15) Feller, S. E.; Gawrisch, K.; MacKerell, A. D. Polyunsaturated Fatty Acids in Lipid Bilayers: Intrinsic and Environmental Contributions to Their Unique Physical Properties. *Journal of the American Chemical Society* **2002**, *124*, 318–326, PMID: 11782184.

(16) Eldho, N. V.; Feller, S. E.; Tristram-Nagle, S.; Polozov, I. V.; Gawrisch, K. Polyunsaturated Docosahexaenoic vs Docosapentaenoic AcidDifferences in Lipid Matrix Properties from the Loss of One Double Bond. *Journal of the American Chemical Society* **2003**, *125*, 6409–6421, PMID: 12785780.

(17) Wohlert, J.; Edholm, O. Dynamics in atomistic simulations of phospholipid membranes: Nuclear magnetic resonance relaxation rates and lateral diffusion. *The Journal of Chemical Physics* **2006**, *125*, 204703.

(18) Klauda, J. B.; Roberts, M. F.; Redfield, A. G.; Brooks, B. R.; Pastor, R. W. Rotation of Lipids in Membranes: Molecular Dynamics Simulation, 31P Spin-Lattice Relaxation, and Rigid-Body Dynamics. *Biophysical Journal* **2008**, *94*, 3074–3083.

(19) Leftin, A.; Brown, M. F. An NMR database for simulations of membrane dynamics. *Biochimica et Biophysica Acta (BBA) - Biomembranes* **2011**, *1808*, 818 – 839, Including the Special Section: Protein translocation across or insertion into membranes.

(20) Klauda, J. B.; Eldho, N. V.; Gawrisch, K.; Brooks, B. R.; Pastor, R. W. Collective and Noncollective Models of NMR Relaxation in Lipid Vesicles and Multilayers. *The Journal of Physical Chemistry B* **2008**, *112*, 5924–5929, PMID: 18179193.

(21) Pastor, R. W.; Venable, R. M.; Karplus, M.; Szabo, A. A simulation based model of NMR T1 relaxation in lipid bilayer vesicles. *The Journal of Chemical Physics* **1988**, *89*, 1128–1140.

(22) Catte, A.; Girych, M.; Javanainen, M.; Loison, C.; Melcr, J.; Miettinen, M. S.; Monticelli, L.; Mtt, J.; Oganesyan, V. S.; Ollila, O. H. S. et al. Molecular electrometer and binding of cations to phospholipid bilayers. *Phys. Chem. Chem. Phys.* **2016**, *18*, 32560–32569.

(23) Ollila, S.; Hyvönen, M. T.; Vattulainen, I. Polyunsaturation in Lipid Membranes: Dynamic Properties and Lateral Pressure

Profiles. *J. Phys. Chem. B* **2007**, *111*, 3139–3150.

(24) Ollila, O. H. S.; Ferreira, T.; Topgaard, D. MD simulation trajectory and related files for POPC bilayer (Berger model delivered by Tieleman, Gromacs 4.5). 2014; {http://dx.doi.org/10.5281/zenodo.13279}.

(25) Klauda, J. B.; Venable, R. M.; Freites, J. A.; O'Connor, J. W.; Tobias, D. J.; Mondragon-Ramirez, C.; Vorobyov, I.; Jr, A. D. M.; Pastor, R. W. Update of the CHARMM All-Atom Additive Force Field for Lipids: Validation on Six Lipid Types. *J. Phys. Chem. B* **2010**, *114*, 7830–7843.

(26) Santuz, H. MD simulation trajectory and related files for POPC bilayer (CHARMM36, Gromacs 4.5). 2015; http://dx.doi.org/10.5281/zenodo.14066, DOI: 10.5281/zenodo.14066.

(27) Antila, H. . 2018; http://dx.doi.org/10.5281/zenodo.148560, DOI: 10.5281/zenodo.1468560.

(28) Kulig, W.; Jurkiewicz, P.; Olżyńska, A.; Tynkkynen, J.; Javanainen, M.; Manna, M.; Rog, T.; Hof, M.; Vattulainen, I.; Jungwirth, P. Experimental determination and computational interpretation of biophysical properties of lipid bilayers enriched by cholesteryl hemisuccinate. *Biochim. Biophys. Acta* **2015**, *1848*, 422 – 432.

(29) Javanainen, M. POPC/Cholesterol @ 310K. 0, 10, 40, 50 and 60 mol-cholesterol. Model by Maciejewski and Rog. **2015**,

(30) Dickson, C. J.; Madej, B. D.; Skjevik, . A.; Betz, R. M.; Teigen, K.; Gould, I. R.; Walker, R. C. Lipid14: The Amber Lipid Force Field. *J. Chem. Theory Comput.* **2014**, *10*, 865–879.

(31) Ollila, O. H. S.; Retegan, M. MD simulation trajectory and related files for POPC bilayer (Lipid14, Gromacs 4.5). 2014; DOI: 10.5281/zenodo.12767.

(32) Jämbeck, J. P. M.; Lyubartsev, A. P. An Extension and Further Validation of an All-Atomistic Force Field for Biological Membranes. *J. Chem. Theory Comput.* **2012**, *8*, 2938–2948.

(33) Javanainen, M. POPC with 0, 10, 20, and 30 mol-Slipids force field. 2016; http://dx.doi.org/10.5281/zenodo.3243328.

(34) Höltje, M.; Förster, T.; Brandt, B.; Engels, T.; von Rybinski, W.; Höltje, H.-D. Molecular dynamics simulations of stratum corneum lipid models: fatty acids and cholesterol. *Biochim. Biophys. Acta* **2001**, *1511*, 156 – 167.

(35) Ollila, O. H. S. MD simulation trajectory and related files for POPC/cholesterol (50 molmodified Hltje, Gromacs 4.5). **2014**,

(36) Lim, J. B.; Rogaski, B.; Klauda, J. B. Update of the Cholesterol Force Field Parameters in CHARMM. *J. Phys. Chem. B* **2012**, *116*, 203–210.

(37) Santuz, H. MD simulation trajectory for POPC/50% Chol bilayer (CHARMM36, Gromacs 4.5). 2015; http://dx.doi.org/10.5281/zenodo.14068, DOI: 10.5281/zenodo.14068.

(38) Jämbeck, J. P. M.; Lyubartsev, A. P. Another Piece of the Membrane Puzzle: Extending Slipids Further. *Journal of Chemical Theory and Computation* **2013**, *9*, 774–784, PMID: 26589070.

(39) Ollila, O. H. S. MD simulation trajectory and related files for POPC bilayer in low hydration (Berger model delivered by Tieleman, Gromacs 4.5). **2015**,

(40) Kanduc, M.; Schneck, E.; Netz, R. R. Hydration Interaction between Phospholipid Membranes: Insight into Different Measurement Ensembles from Atomistic Molecular Dynamics Simulations. *Langmuir* **2013**, *29*, 9126–9137.

(41) Kanduc, M. MD trajectory for DLPC bilayer (Berger, Gromacs 4.5.4), nw=16 w/l. 2015; DOI: 10.5281/zenodo.16292.

(42) Kanduc, M. MD trajectory for DLPC bilayer (Berger, Gromacs 4.5.4), nw=12 w/l. 2015; DOI: 10.5281/zenodo.16293.

(43) Ollila, O. H. S.; Miettinen, M. MD simulation trajectory and related files for POPC bilayer in medium low hydration (CHARMM36, Gromacs 4.5). 2015; {http://dx.doi.org/10.5281/zenodo.13946}, DOI: 10.5281/zenodo.13946.

(44) Ollila, O. H. S.; Miettinen, M. MD simulation trajectory and related files for POPC bilayer in low hydration (CHARMM36, Gromacs 4.5). 2015; {http://dx.doi.org/10.5281/zenodo.13945}, DOI: 10.5281/zenodo.13945.

(45) Javanainen, M. POPC @ 310K, varying water-to-lipid ratio. Model by Maciejewski and Rog. 2014; {http://dx.doi.org/10.5281/zenodo.13498}, DOI: 10.5281/zenodo.13498.

(46) Venable, R. M.; Luo, Y.; Gawrisch, K.; Roux, B.; Pastor, R. W. Simulations of Anionic Lipid Membranes: Development of Interaction-Specific Ion Parameters and Validation Using NMR Data. *J. Phys. Chem. B* **2013**, *117*, 10183–10192.

(47) Ollila, O. H. S. MD simulation trajectory and related files for POPC bilayer with 350mM NaCl (CHARMM36, Gromacs 4.5). 2015; http://dx.doi.org/10.5281/zenodo.32496.

(48) Ollila, O. H. S. MD simulation trajectory and related files for POPC bilayer with 690mM NaCl (CHARMM36, Gromacs 4.5). 2015; http://dx.doi.org/10.5281/zenodo.32497.

(49) Ollila, O. H. S. MD simulation trajectory and related files for POPC bilayer with 950mM NaCl (CHARMM36, Gromacs 4.5). 2015; http://dx.doi.org/10.5281/zenodo.32498.

(50) Åqvist, J. Ion-water interaction potentials derived from free energy perturbation simulations. *J. Phys. Chem.* **1990**, *94*, 8021–8024.

(51) Javanainen, M.; Tynkkynen, J. POPC @ 310K, varying amounts of NaCl. Model by Maciejewski and Rog. 2015; http://dx.doi.org/10.5281/zenodo.14976.

(52) Smith, D. E.; Dang, L. X. Computer simulations of NaCl association in polarizable water. *J. Chem. Phys* **1994**, *100*, 3757–3766.

(53) Javanainen, M. POPC @ 310K, 130 mM of NaCl. Slipids with ions by Smith & Dang. 2015; http://dx.doi.org/10.5281/zenodo.35275.

(54) Javanainen, M. POPC with varying amounts of cholesterol, 1 M of NaCl. Slipids with ions by Smith & Dang. 2015; http://dx.doi.org/10.5281/zenodo.259341.

(55) Schlenkrich, M.; Brickmann, J.; MacKerell, A. D.; Karplus, M. *Biological Membranes*; Springer, 1996; pp 31–81.

(56) Feller, S. E.; MacKerell, A. D. An improved empirical potential energy function for molecular simulations of phospholipids. *The Journal of Physical Chemistry B* **2000**, *104*, 7510–7515.

(57) Pham, Q. D.; Topgaard, D.; Sparr, E. Cyclic and Linear Monoterpenes in Phospholipid Membranes: Phase Behavior, Bilayer Structure, and Molecular Dynamics. *Langmuir* **2015**, *31*, 11067–11077, PMID: 26375869.

(58) Seelig, J.; MacDonald, P. M.; Scherer, P. G. Phospholipid head groups as sensors of electric charge in membranes. *Biochemistry* **1987**, *26*, 7535–7541, PMID: 3322401.

Graphical TOC Entry

TOC here if needed